Controlled Ablation of Microtubules Using a Picosecond Laser

E. L. Botvinick,*† V. Venugopalan,*‡ J. V. Shah,§ L. H. Liaw,* and M. W. Berns*†¶

*Beckman Laser Institute, University of California, Irvine, Irvine, California; †Department of Bioengineering, University of California, San Diego, La Jolla, California; ‡Department of Chemical Engineering and Materials Science, University of California, Irvine, Irvine, California; §Ludwig Institute for Cancer Research, University of California, San Diego, La Jolla, California; and ¶Department of Biomedical Engineering, University of California, Irvine, Irvine, California

ABSTRACT The use of focused high-intensity light sources for ablative perturbation has been an important technique for cell biological and developmental studies. In targeting subcellular structures many studies have to deal with the inability to target, with certainty, an organelle or large macromolecular complex. Here we demonstrate the ability to selectively target microtubule-based structures with a laser microbeam through the use of enhanced yellow fluorescent protein (EYFP) and enhanced cyan fluorescent protein (ECFP) variants of green fluorescent protein fusions of tubule. Potorous tridactylus (PTK2) cell lines were generated that stably express EYFP and ECFP tagged to the α-subunit of tubulin. Using microtubule fluorescence as a guide, cells were irradiated with picosecond laser pulses at discrete microtubule sites in the cytoplasm and the mitotic spindle. Correlative thin-section transmission electron micrographs of cells fixed one second after irradiation demonstrated that the nature of the ultrastructural damage appeared to be different between the EYFP and the ECFP constructs suggesting different photon interaction mechanisms. We conclude that focal disruption of single cytoplasmic and spindle microtubules can be precisely controlled by combining laser microbeam irradiation with different fluorescent fusion constructs. The possible photon interaction mechanisms are discussed in detail.

INTRODUCTION

More than 30 years ago it was demonstrated that a microsecond-pulsed argon ion laser could be focused to a diffraction-limited spot for subcellular microsurgery of chromosomes (Berns et al., 1969). Subsequent studies on mitotic structures (spindle poles, chromosomes, and kinetochores; McNeill and Berns, 1981), mitochondria, and actin stress fibers demonstrated a general utility of this approach for the study of cell structure and function (Berns et al., 1981). In those early experiments, either light-sensitizing vital dyes were used to create subcelluar sensitivity to the light, or nanosecond-pulsed lasers were used to produce effects without the use of an external sensitizing agent. It was suggested that the effects produced by the nanosecond laser were due to multiphoton absorption (Berns, 1976; Calmettes and Berns, 1983). Since that time structural and functional studies have been conducted on a wide variety of cellular and developmental problems (Aist et al., 1993; Grill et al., 2001; Khodjakov et al., 1997a; Liang et al., 1993, 1994; Rieder et al., 1995; Skibbens et al., 1995; Spurck et al., 1990) including the use of dye-mediated multiphoton-induced chemistry to inactivate the nucleolar genes in live cells (Berns et al., 2000). Additionally recent studies employing femtosecond-pulsed lasers suggest significant nonlinear interactions with biological material (Joglekar et al., 2004; Tirlapur and Konig, 2002). However, a major limitation in much of this work has been the inability to clearly visualize and then manipulate the target structures, many of which are either at or below the resolution of the light microscope.

The combination of subcellular laser ablation with the use of gene fusion products permits the visualization and alteration of cellular structures that are below the resolution of the light microscope (Khodjakov et al., 1997b). The ability to visualize and target organelles of increasingly smaller size has the potential of greatly expanding the application of subcellular surgery. Paralleling the development of these new molecular tools, have been advances in laser technology resulting in lasers with pulses of increasingly shorter duration that have the potential to provide for finer and more subtle effects. The photo-physical events that occur within a diffraction-limited volume of a living cell, and the nature and extent of the induced changes are not well understood. In this article we describe the use of picosecond laser pulses in combination with two tubulin fusion proteins to visualize and cleanly ablate (cut) microtubules in mitotic and interphase cells. The nature and structure of the alteration sites in individual cells are examined by serial thin-section transmission electron microscopy (TEM) and the possible physical mechanisms responsible for the ablation process are discussed.

METHODS

Software

Software for computer control of all hardware and image acquisition was custom coded in the LabVIEW (National Instruments, Austin, TX) programming language. Images were prepared for publication using Adobe Photoshop and ImageJ (http://rsb.info.nih.gov/ij).

Submitted July 13, 2004, and accepted for publication September 17, 2004.

Address reprint requests to Michael W. Berns, 1002 Health Sciences Rd., East Irvine, CA 92612. Tel.: 949-824-7565; Fax: 949-824-8413; E-mail: mberns@bli.uci.edu.

0006-3495/04/12/4203/10 $2.00

doi: 10.1529/biophysj.104.049528

Constructs and cell lines

Cells and methods of cell culture used in these studies were from established sublines of rat kangaroo (*Potorous tridactylus)* kidney epithelium, PTK2 (Berns and Floyd, 1971; Liang and Berns, 1983; McNeill and Berns, 1981; Walen and Brown, 1962). Generation of cell lines stably expressing fluorescent protein fusions of human α-tubulin were generated by amphotropic retroviral infection. The human α-tubulin cDNA fused at its N-terminus to the enhanced yellow variant of green fluorescent protein (EYFP) was excised from a commercially available plasmid (Clontech, Palo Alto, CA) via an AfeI/MfeI digest. This fragment was ligated into the *Sna*BI/*Eco*RI sites of pBABEbsd, a retroviral vector based on pBABEpuro (Morgenstern and Land, 1990) with a blasticidin resistance marker. The cyan version of the tubulin fusions (ECFP-α-tubulin) was generated by the insertion of the α-tubulin cDNA into the ECFP-C1 vector (Clontech) and then excised by AfeI/MfeI and inserted into a pBABEpuro.

The retroviral plasmids containing the fluorescent protein-tubulin fusions were cotransfected, using the Fugene transfection reagent (Roche Applied Sciences, Indianapolis, IN), into 293-GP cells (a human embryonic kidney cell line harboring a portion of the Murine Moloney Leukemia Virus genome) along with a VSV-G pseudotyping plasmid to generate amphotropic virus. Forty-eight hours after transfection, the tissue culture supernatant was collected, filtered, and 10% of the total filtrate placed onto a subconfluent culture (30–40%) of PTK2 cells in 35-mm dishes. Forty-eight hours after infection, cells were split and replated in 10-cm dishes and subjected to selection in 2 μg/mL puromycin (ECFP-tubulin) or 2 μg/mL blasticidin (EYFP-tubulin) for 14 days. High expressors (top 10%) were selected by fluorescence-activated cell sorting (FACS, FACSVantage, Becton Dickinson, San Jose, CA). Cells were maintained as polyclonal lines exhibiting various levels of tubulin expression.

Laser scissors (ablation) system

The laser scissors system is shown in Fig. 1. The second harmonic ($\lambda = 532$ nm) laser line from a mode-locked Nd-YAG laser emitting 80-ps pulses at 76 MHz was used for laser ablation (Antares laser; Coherent, Santa Clara, CA). Laser power was controlled via a Glan laser linear polarizer (CVI Laser, Albuquerque, NM) mounted in a motorized stepper rotary mount (New Focus, San Jose, CA). The attenuated laser beam was sampled via partial reflection off a mounted glass coverslip onto a large-area photodiode (New Focus) to provide laser power feedback measurements. A motorized mechanical shutter (Vincent Associates, Rochester, NY) provided 3-ms exposures (containing 228,000 individual ps pulses) of the laser output into the microscope. Custom software monitored photodiode output, rotated the polarizer, and opened/closed the shutter to provide closed loop control of laser power and exposure times. Standard epifluorescence optics were removed from the microscope and an external lens system focused the arc lamp light into the microscope objective lens. A motorized flip-mirror mount (New Focus) could be programmatically either inserted or removed from the optical path. Shuttered laser light was expanded (3X expander; Newport, Irvine, CA), and elevated to the height of the epifluorescence light port of the microscope by precision beam splitters (Newport). The beam was reflected into the microscope with a dielectric mirror (Newport) mounted in the motorized flip-mirror mount so that laser light would be reflected, unaltered by microscope lenses, by a dielectric mirror mounted in the dichroic-mirror slot of the microscope fluorescence cube slider (Chroma Technology, Brattleboro, VT). Reflected light entered the back aperture of a Zeiss 63X PH3 numerical aperture 1.4 oil-immersion objective lens used for both laser ablation and imaging. The mercury arc lamp was removed from the microscope body and repositioned further away from the microscope. Auxiliary lenses were used to refocus the image of the arc onto the back image plane of the microscope objective. When the flip mirror was down, arc lamp light was focused by those lenses and reflected by the appropriate filter cube (Chroma) into the objective lens. A shutter (Vincent Associates) was controlled by the computer for arc lamp exposure. Fluorescence images were collected using a high-sensitivity Quantix 57 back-illuminated charge-coupled device camera (Roper Scientific, Trenton, NJ).

Energy measurements were made by calibrating the photodiode output to laser power measured in the specimen plane. To estimate laser power in the specimen plane, laser output from the objective lens was recollected onto a precalibrated laser light meter (Newport). A calibration curve was generated from repeated measurements at a range of powers to convert the photodiode output (V) (from the sampled beam) into laser average power in the specimen plane (W). Energy per pulse was estimated as average power divided by pulse-repetition rate. Energy per unit area was estimated by assuming the area of focus was the area of the theoretical Airy disk

$$r_s = \frac{0.61\lambda}{NA_{obj}}, \tag{1}$$

where λ is 532 nm, and $NA_{obj} = 1.4$ is the numerical aperture of the objective lens. The laser shutter provided 3-ms exposures of the laser output so that total energy for each 3-ms exposure can be estimated by multiplying the energy per pulse by the product of repetition rate and exposure duration. For clarity we will refer to each individual 80-ps laser pulse as a micropulse and each 3-ms exposure of pulses as a macropulse.

TEM procedures

Serial thin-section (60 nm per slice) transmission electron microscopy (TEM) of single irradiated cells was carried out using previously described procedures (Liaw and Berns, 1981). Crucial to these experiments was the fixation of cells for TEM within 1 s of laser exposure. To accomplish this, two 23-gauge syringe needles were inserted through the Rose chamber silicone gasket. One needle served as an exit needle and the other as the input needle for the fixative solution. The chamber containing a near-confluent monolayer of PTK2 cells was placed under the laser microscope and a suitable cell for study was located and digitally recorded using both phase contrast and fluorescence microscopy. Initially cell images were taken using combined phase and fluorescence microscopy. A second fluorescence image immediately before laser exposure was taken, and a third fluorescence image was taken immediately after laser exposure. Three milliliters of fixative was injected into the chamber within 1 s of the last fluorescence image and the cell was processed for TEM analysis. Twenty-three cells were irradiated, fixed, and serial sectioned for TEM analysis.

RESULTS

Laser energy ablation thresholds for EYFP and ECFP were determined by irradiating the midregion of individual cytoplasmic microtubules in interphase cells. To determine that the loss of fluorescence was a real cut/break in the microtubules as opposed to photobleaching, a digital time-lapse series of microtubule behavior was made after each macropulse exposure. The directional lengthening (polymerization), shortening (depolymerization), and/or deformation of the irradiated single microtubule at or near the ablation site was used as the criterion for a cut. Otherwise we assumed loss of fluorescence is due to photobleaching of the fluorescent moiety (Fig. 2). The thresholds for ablation of the two probes were: ECFP, 0.18 nJ/micropulse, corresponding to a macropulse radiant exposure of 0.106 J/cm^2, and for EYFP, 0.01 nJ/micropulse, corresponding to a macropulse radiant exposure of 0.0059 J/cm^2. Precise focal ablation (cutting) of the microtubules was confirmed by transmission electron microscopy (see description given below).

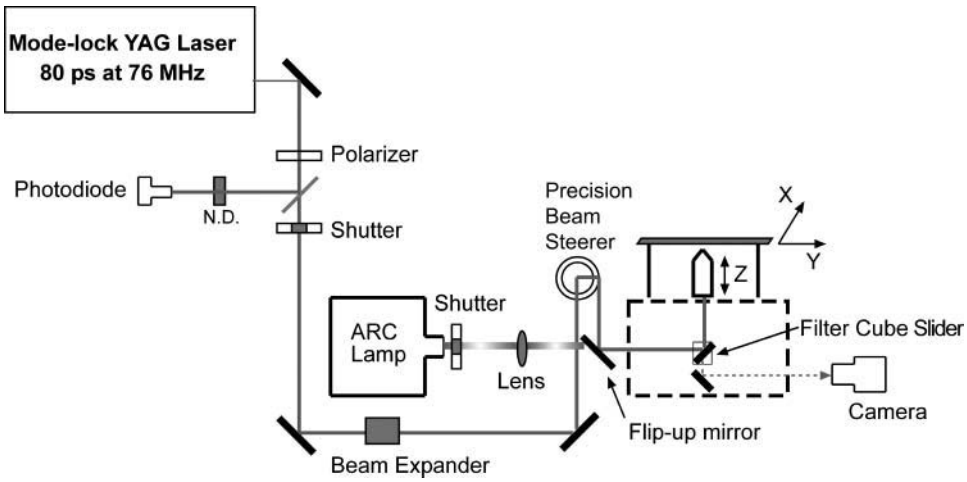

FIGURE 1 The laser ''scissors'' system. The second harmonic ($\lambda = 532$ nm) laser line from a mode-locked Nd-YAG laser emitting 80-ps pulses at 76 MHz was used for laser ablation. The beam was sampled by a photodiode after partial reflection off a glass coverslip and attenuation by a neutral density filter (*N.D.*). A shutter provided 3-ms exposures, or macropulses, comprised of 228,000 individual pulses, or micropulses. A flip-up mirror mount and externalized epifluorescence optics allowed both the laser and arc lamp light into the back of the microscope. The filter cube slider holds cubes for EYFP and ECFP imaging, and for reflecting the laser light into the microscope objective. A high-sensitivity camera recorded fluorescence and phase contrast images before and after each irradiation.

Spindle microtubules are usually visualized in discrete bundles (spindle fibers) of microtubules that either terminate at the chromosome, or extend from pole to pole. In these studies, individual chromosome spindle fibers were irradiated at a point between the spindle pole and the chromosome in EYFP cells (Fig. 3) and in ECFP cells (Fig. 4). This was possible because the cell was first observed (and recorded) simultaneously by phase contrast and fluorescence microscopy. Thus, a spindle fiber attached to a specific chromosome could be targeted (Figs. 3, *A–C*, and 4, *A–C*).

The ultrastructural alterations using the EYFP probe were very precise and demonstrated little, if any, collateral damage outside the focal point (Fig. 3, *D–F*). Delivery of a 6.74×10^4 J/cm^2 macropulse (0.5 nJ/micropulse) to the focal volume resulted in a loss of fluorescence (Fig. 3 *C*, *arrow*) and a corresponding loss of microtubule ultrastructure (Fig. 3, *D–F*). The gap between the two ends of the severed spindle fiber is determined from TEM to be 0.34 μm (Fig. 3). From Eq. 1, the calculated Airy disk diameter of the focused laser spot provided by the microscope objective used is 0.46 μm.

The results with ECFP were significantly different from those for EYFP. To provide for microtubule scission, the micropulse energy for ECFP ablations had to be increased to 0.92 nJ/pulse resulting in a macropulse radiant exposure of 1.24×10^5 J/cm^2. The subsequent ultrastructural alterations were also different from those observed at lower energy using EYFP (Fig. 4, *D–F*). Within the ablation zone, small vesicles/vacuoles (0.3-μm diameter) were observed. These vesicles/vacuoles were seen to have individual microtubules attached to them with a very distinct zone of slightly increased electron density associated with the attachment site (Fig. 4 *F*). Serial sections above and below revealed that the vesicles occupied three sections (60 nm/section). The

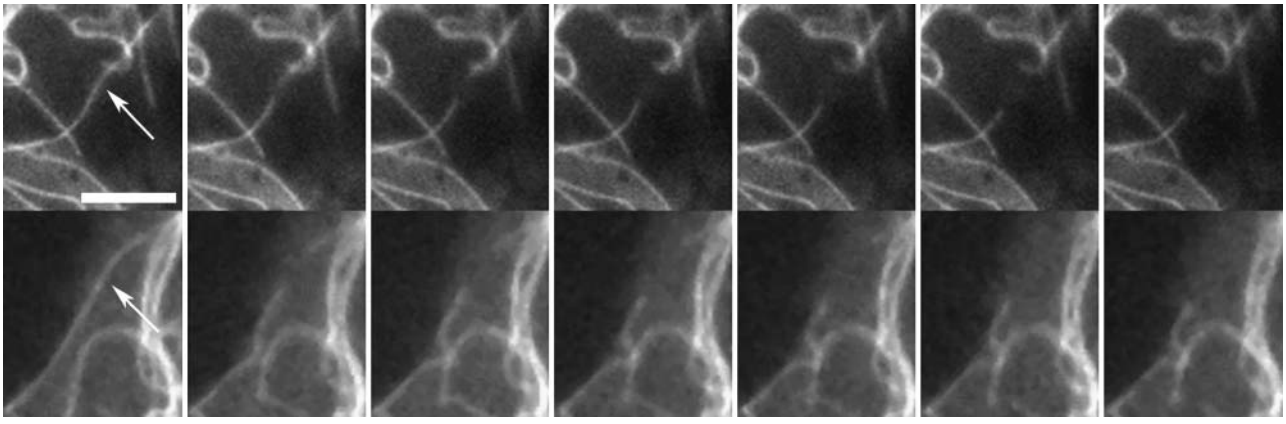

FIGURE 2 Individual cytoplasmic microtubule ablation. Two individual ECFP-labeled microtubules in interphase cells irradiated at supra-threshold irradiances. Arrows indicate irradiation target. The newly formed microtubule fragments can be seen depolymerizing. (*Top*) 8 s between frames; (*bottom*) 4 s between frames. Scale bar = 10 μm.

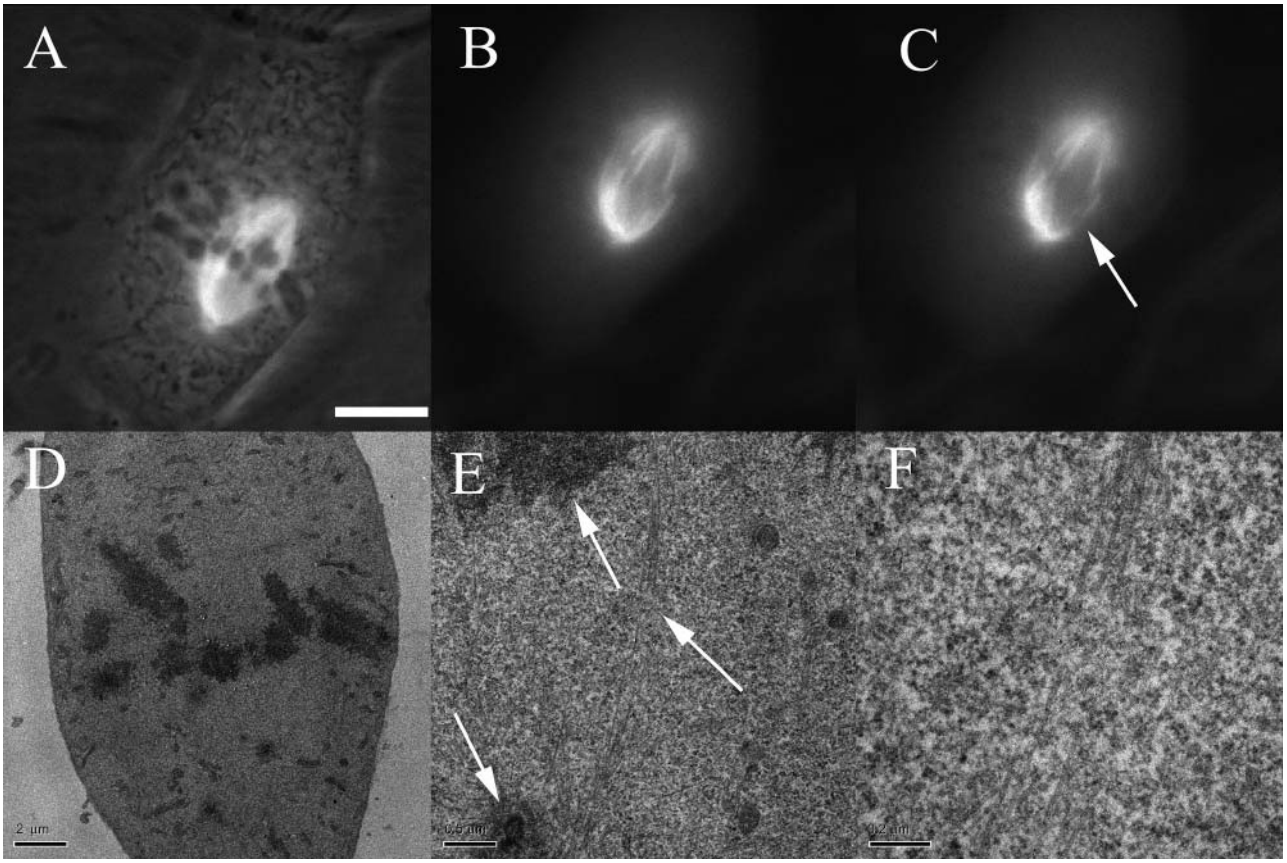

FIGURE 3 Spindle cutting with EYFP probe. (*A*) Combined phase contrast and EYFP fluorescence of metaphase cell; (*B*) fluorescent image before irradiation; (*C*) postirradiation to microtubule bundle (*arrow*); 0.5 nJ/micropulse; total 6.74×10^4 J/cm^2 per macropulse; (*D*) low magnification TEM of cell fixed <5 s postirradiation; (*E*) medium magnification TEM illustrating cut zone, pole, and chromosome (*arrows*); (*F*) high magnification TEM illustrating cleanly cut microtubules in the cut zone. (*A–C*) Scale bar = 10 μm. (*D–F*) Scale bar = 2, 0.5, 0.2 μm, respectively.

cytoplasm in the *x*, *y*, and *z* axes around the vesicles appeared to contain microtubule fragments.

Fig. 5 demonstrates centriole ablation in which the locations of the two centrosomes of a mitotic cell were inferred from the EYFP labeling of the microtubules (Fig. 5, *A–C*). Fluorescent images were acquired before ablation (Fig. 5 *A*; combined with phase contrast), immediately postablation (Fig. 5 *B*), and 15 min postablation (Fig. 5 *C*). The micropulse energy was 0.66 nJ/pulse with a macropulse radiant exposure of 8.90×10^4 J/cm^2. TEM shows the intact pair of centrioles in the lower, unablated centrosome (Fig. 5 *E*) and the altered pair of centrioles in the upper irradiated centrosome (Fig. 5 *F*). The pericentriolar material appears intact for the irradiated centrosome that could account for the return of the fluorescent spindle in Fig. 5 *C*.

DISCUSSION

Using EYFP and ECFP it is possible to produce controlled damage in mitotic spindle fibers and individual cytoplasmic microtubules. In the case of the EYFP spindle, a detectable loss in fluorescence followed a successful ablation of the microtubules, and under TEM there was no visible alteration other than the gap between the microtubules in the severed bundle. The gap under TEM is 0.3-μm wide, smaller than the Airy disk diameter, whereas the gap under fluorescence appears wider and is probably due to photobleaching of neighboring fluorescent molecules. The EYFP-tubulin spindle microtubules appeared to be cleanly severed with no ultrastructural debris evident in or around the ablation area. Because the cell chambers were set up under the microscope with a perfusion system, it was possible to inject fixative into the culture chamber within one second of laser exposure thus mitigating subsequent structural changes and diffusion of material out of or into the irradiation zone.

When ablating ECFP-tubulin spindle microtubules we found that a detectable loss in fluorescence, using standard epifluorescence, did not necessarily correspond to ablation of the microtubules. With the EYFP-tubulin it is likely that photobleaching of molecules adjacent to the ablation site contributes to the change in contrast at the laser focus after ablation. It appears that with the ECFP tubulin, the adjacent

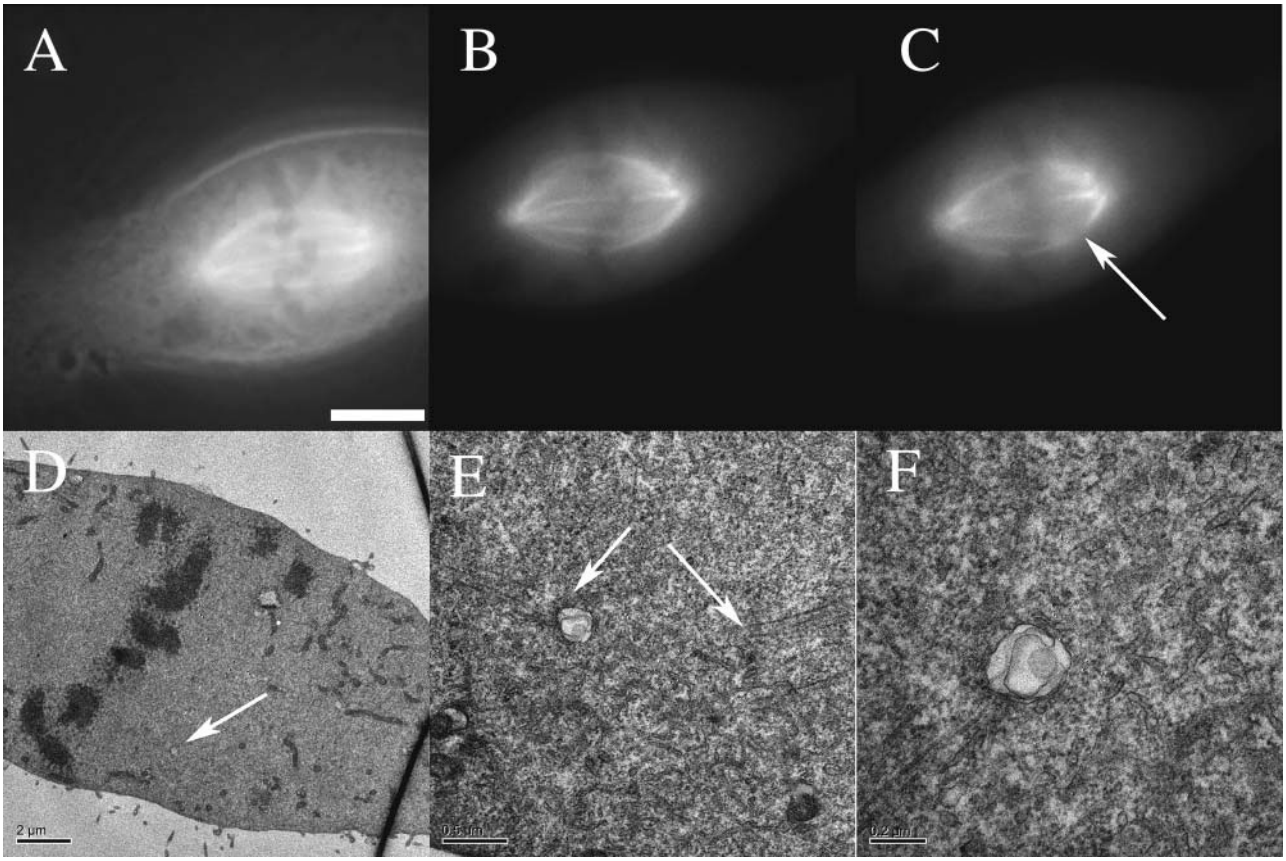

FIGURE 4 Supra-threshold spindle cutting with ECFP probe. (*A*) Combined phase contrast and ECFP fluorescence of metaphase cell; (*B*) fluorescent image before irradiation; (*C*) postirradiation to microtubule bundle (*arrow*); two consecutive macropulses; 0.92 nJ/micropulse, 1.24×10^5 J/cm^2 per macropulse; (*D*) low magnification TEM of cell fixed <5 s postirradiation; note vacuole (*arrow*); (*E*) medium magnification TEM illustrating ends of cut microtubule bundle (*arrows*); (*F*) high magnification of ablation zone; note microtubules truncated at 0.2-μm diameter vacuole. (*A–C*) Scale bar = 10 μm. (*D–F*) Scale bar = 2, 0.5, 0.2 μm, respectively.

molecules were not photobleached, and the resulting subresolution ablation is masked by the spreading fluorescence of neighboring molecules. When the micropulse energy was increased to a level where fluorescence loss was detected, lesions of the ECFP-tubulin cells, as seen in TEM, were slightly wider than the laser focal spot (1.4 μm in diameter) and some cut microtubules appeared to be attached to small vesicles. There also seemed to be some electron dense material associated with this region. Other microtubules in this region appeared to be cleanly severed without any associated vesicles or electron dense material.

The appearance of the damage of the EYFP and ECFP cells reported here is substantially different than that reported for green fluorescent protein (GFP) cells by Khodjakov et al. (1997b). In that review the high-voltage TEM of 0.5-μm- and 0.25-μm-thick sections of laser-targeted GFP-spindle fibers and GFP centrosomes were described. The subcellular targets were exposed to 3–4 s of nanosecond pulses of the 532-nm beam of a frequency doubled Nd-YAG laser operating at 10 Hz. The micropulse energies in the specimen plane were estimated to be 300–600 nJ. The ultrastructural damage to the microtubules is described as an ''electron dense track of denatured protein'' termed ''sniglets''. Ultrastructural damage to the centrosomes is described as ''...an electron-opaque mass of denatured protein''. In more recent articles (Khodjakov et al., 2002), they describe complete destruction of centrosomes by repeated movement of the microscope in the *x*, *y*, and *z* axes while exposing the structures to two to three series of 20–30 laser pulses over a 10-s period. The laser-induced damage is described as electron-opaque denatured protein. In those studies it is possible that the initial laser pulses altered the absorption properties of the target so that subsequent exposure as the beam was moved repeatedly through the *x*, *y*, and *z* axes resulted in single-photon absorption and subsequent heat generation resulting in the denaturation of the material. It is difficult to make meaningful comparisons between studies retrospectively because laser parameters as well as cell exposure conditions differ widely. In this study, we delivered 80-ps laser pulses at a repetition rate of 76 MHz as opposed to 10-ns laser pulses delivered at 10 Hz (Calmettes and Berns, 1983), or

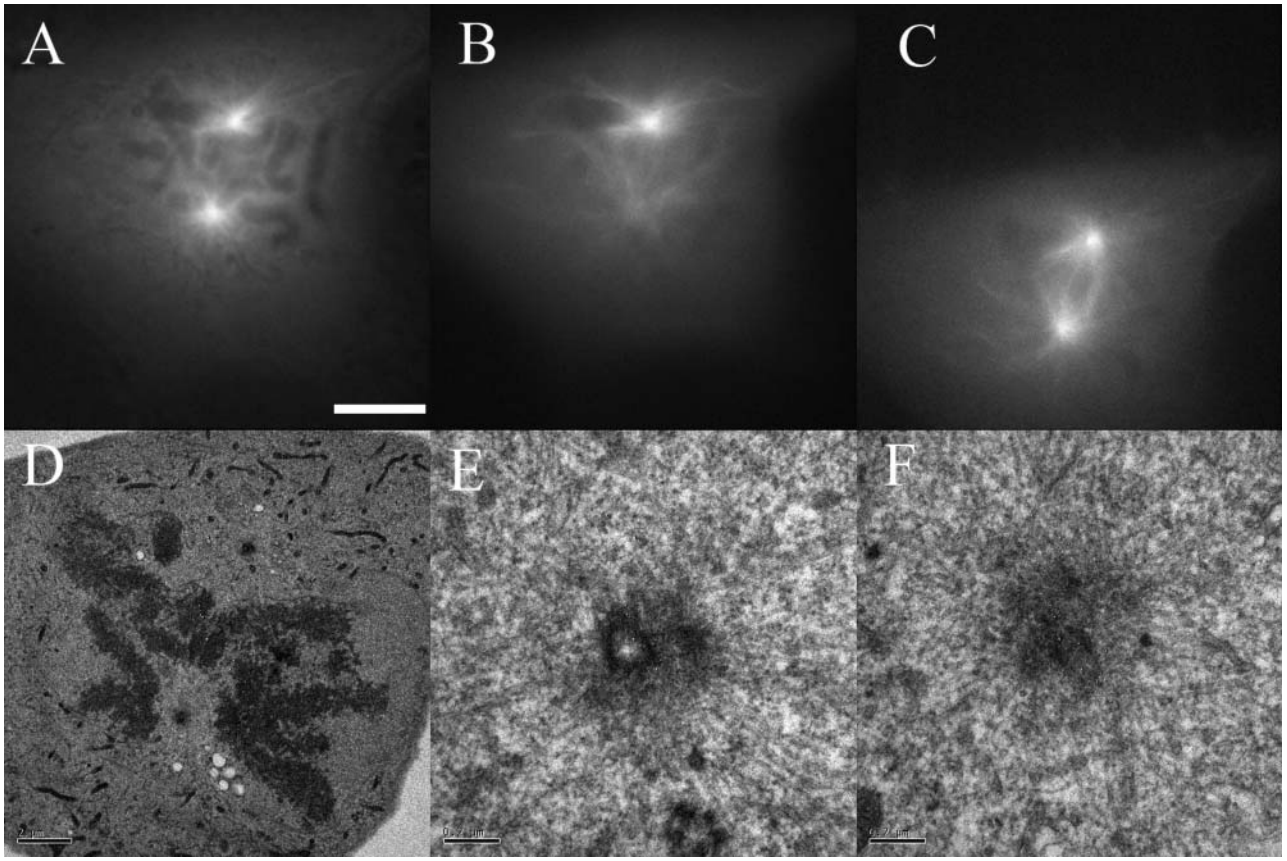

FIGURE 5 Centriole cutting with EYFP probe. (*A*) Combined phase contrast and fluorescence of metaphase cell expressing EYFP-tubulin at both poles; (*B*) fluorescent image ~2 s postirradiation; 0.66 nJ/micropulse, total 8.90×10^4 J/cm^2 per macropulse; (*C*) recovery of fluorescence 15 min postirradiation; (*D*) low-magnification TEM of cell fixed >15 min postirradiation ; (*E*) TEM of unexposed centrosome illustrating tubular structure of centrioles; (*F*) irradiated centrosome illustrating amorphous altered structure of centrioles; Both poles have normal appearing pericentriolar material and microtubule nucleation. (*A–C*) Scale bar = 10 μm. (*D–F*) Scale bar = 2, 0.5, 0.2 μm, respectively.

microsecond laser pulses (Berns and Floyd, 1971; Berns et al., 1969) as employed in early studies.

In general we must consider four potential mechanisms for the production of damage to the target structure: a), temperature rise produced by the linear absorption; b), temperature rise due to multiphoton absorption; c), generation of large thermoelastic stresses; and d), thermal, mechanical, and chemical processes emanating from optical breakdown (plasma formation) produced by a combination of multiphoton and cascade ionization processes.

The linear optical absorption properties of the microtubules examined in this study are governed by the absorption spectra and concentrations of the EYFP and ECFP probes. To calculate the concentration of the probe molecule in the microtubule we assume that a single EYFP/ECFP probe molecule is attached to every α-β tubulin subunit. This serves as an upper bound because the endogenous molecules will compete with exogenous molecules during the polymerization of microtubules. With this assumption, the knowledge of the molecular weights of the probe molecules and the α-β tubulin subunit (99,948.92 g/mol), and the mass density of a microtubule (0.757 g/cm^3) we determine the concentration of these probes in the microtubule to be 1.266 mM. With this concentration and the molar absorption coefficients of ECFP and EYFP at $\lambda = 532$ nm being 95 and 11,524 cm^{-1} M^{-1}, respectively (determined with a Beckman DU650 spectrophotometer), we find that the absorption coefficients of the ECFP- and EYFP-tagged microtubules at $\lambda = 532$ nm to be $\mu_a = 0.2769$ cm^{-1} and 33.59 cm^{-1}, respectively. Thus, the linear absorption by the EYFP-tagged microtubule exceeds the ECFP-tagged microtubule by more than 120-fold.

With these values for the absorption coefficient we must determine the radiant exposure incident on the microtubule. We consider the radiant exposure produced at threshold by a single 80-ps micropulse. The threshold micropulse energy necessary to produce damage was 0.18 nJ and 0.01 nJ for the ECFP- and EYFP-tagged microtubules, respectively. Assuming that the laser beam was focused to a diffraction-limited spot as estimated by Eq. 1 we find that the threshold micropulse energies are equivalent to threshold radiant exposures of 0.106 J/cm^2 and 0.0059 J/cm^2 for ECFP- and

EYFP-tagged microtubules, respectively. These threshold radiant exposures can be converted to temperature rises using the expression:

$$\Delta T = \frac{\mu_a \Phi_0}{\rho c_v}, \tag{2}$$

where μ_a, ρ, and c_v are the absorption coefficient, density, and specific heat (2.3 J/g K) of the microtubule and Φ_0 is the incident radiant exposure (J/cm^2). The temperature rise produced by a single 80-ps micropulse as predicted by Eq. 2 is 0.0169 K and 0.114 K for ECFP- and EYFP-tagged microtubules, respectively. Although these temperature rises are very small and unlikely to produce any damage, we deliver ~228,000 micropulses to the microtubules at 13-ns intervals during the 3-ms macropulse. Thus, we must determine how much cooling occurs during the 13-ns interval between micropulses to assess the temperature rise within the microtubules after the 3-ms macropulse. To get a lower bound for how much cooling we can get between micropulses we assume that there are microtubules placed side by side with one another such that they form a 24-nm-thick microtubule ''sheet'' in the focal plane. We assume that the microtubules are uniformly heated resulting in a temperature rise of ΔT at time = 0. Under such conditions the temperature change in the center of this microtubule sheet as a function of time after the laser pulse $\Delta T(t)$ is given by:

$$\frac{\Delta T(t)}{\Delta T(t=0)} = 1 - \exp(d^2/4\kappa t), \tag{3}$$

where d is the thickness of the slab and κ is the thermal diffusivity (Carslaw and Jaeger, 1986). Such a calculation reveals that only 7.4% (or 0.074) of the initial temperature rise produced by a micropulse is retained before the delivery of the successive micropulse. Denoting the remaining fraction of the initial temperature rise using the variable m ($m = 0.074$ in this case) the temperature rise generated by the delivery of k pulses to the target, ΔT_k is given by:

$$\Delta T_k = \Delta T_0 \sum_{i=1}^{k} m^i = \frac{\Delta T_0}{1-m} \quad \text{as} \quad k \to \infty, \tag{4}$$

where ΔT_0 is the temperature rise produced by the first micropulse. Thus, the maximum temperature that can be expected is $1.08\Delta T_0$ and amounts to 0.0183 K and 0.123 K for ECFP- and EYFP-tagged microtubules, respectively. These temperature rises represent an upper bound for we have modeled the cooling of the microtubule between pulses as the cooling of a slab rather than an isolated cylinder that would cool much faster. Clearly, it is difficult to believe that such temperature rises could produce cutting of the microtubule.

Although these temperature rises are small, the fact that they are generated on a picosecond timescale opens the possibility that significant thermoelastic stresses may be generated (Vogel and Venugopalan, 2003). The significance of thermoelastic stresses can be determined by calculating the stress relaxation factor τ_m that is defined as the ratio of the laser pulse duration t_p to the characteristic time necessary for a stress wave to traverse the heated structure. This latter time is simply the characteristic size of the structure d divided by the speed of sound c_a. Thus, $\tau_m = (t_p\, c_a / d) = 9$ in our case for an 80-ps laser pulse, a 24-nm diameter microtubule, and with an estimate of $c_a = 2600$ m/s. A value of $\tau_m < 1$ signifies that the laser pulse duration is significantly shorter than the time necessary to dissipate thermal stresses. This is known as stress confinement and results in the largest stress amplitudes. In our case, $\tau_m = 9$ and thus the stress magnitudes are not as high. Under these conditions, an estimate for the peak magnitude of thermoelastic stress σ_p is given by

$$\sigma_p = A\Gamma\mu_a\Phi_0, \tag{5}$$

where A is a factor to compensate for the fact that stress confinement is not achieved and takes a value of $A = 0.1$ for $\tau_m = 9$, Γ is the Gruneisen coefficient that we take equal to 1.0 for a polymeric material such as a microtubule (Paltauf and Dyer, 2003), μ_a is the absorption coefficient of the microtubule and Φ_0 is the incident radiant exposure. This computation reveals peak thermoelastic stresses of 3 kPa and 20 kPa for ECFP- and EYFP-tagged microtubules, respectively. Although the yield strength for a microtubule is unknown, recent studies that use optical techniques to measure the rigidity of microtubules indicate that it has mechanical properties similar to polymethylmethacrylate (PMMA), which has a yield strength of 40–70 MPa (Takasone et al., 2002). Thus, it is unlikely that the microtubule is damaged by thermoelastic stresses in the kPa range.

The preceding considerations indicate that the thermomechanical transients generated by linear absorption of the laser energy are unlikely to produce the observed damage of the microtubules. However, given that the micropulses are only 80 ps in duration, the peak irradiances delivered to the microtubule are substantial and opens the possibility that two-photon absorption may be significant. In fact it is well known that in the visible spectrum, the two-photon absorption cross sections of the aromatic amino acid residues tryptophan (Trp), tyrosine (Tyr), and phenylalanine (Phe) are significant (Rehms and Callis, 1993). Thus, a calculation for the amount of two-photon absorption by the microtubule is necessary. Sengupta and co-workers recently measured the two-photon cross section of Trp at $\lambda = 532$ nm to be $\sigma_2 = 32.0 \pm 1.2$ mGM or 0.032×10^{-50} cm^{4}s/photon molecule (Sengupta et al., 2001). Using the relative two-photon absorption spectra published by Rehms and Callis, we can deduce that at $\lambda = 532$ nm, Tyr has a two-photon cross section that is ~10% of this value and that the two-photon cross section of Phe is negligible. To determine the amount of light that may be absorbed we must first examine the

composition of tubulin and EGFP/EYFP with respect to Trp and Tyr. The tubulin dimer contains 996 amino acid residues of which only eight are Trp and 35 Tyr. Taking the sequence of EGFP, which contains 239 amino acid residues, we find only one Trp residue and 11 Tyr. Using the molecular weights of tubulin, EGFP, Trp, and Tyr, we find the mass fractions of Trp and Tyr in the tagged microtubule to be 1.449×10^{-2} and 6.569×10^{-2}, respectively. With these mass fractions, we can compute the two-photon absorption coefficient of Trp or Tyr, $\alpha_2^{\mathrm{Trp/Tyr}}$, in the tagged microtubules using the expression (Bhawalkar et al., 1996)

$$\alpha_2^{\mathrm{Trp/Tyr}} = \frac{\sigma_2^{\mathrm{Trp/Tyr}} N_{\mathrm{A}}}{h\nu} \frac{\rho x^{\mathrm{Trp/Tyr}}}{M}, \tag{6}$$

where $\sigma_2^{\mathrm{TRY/TYR}}$ is the two-photon absorption cross section of Trp or Tyr, N_{A} is the Avogadro number, h is Planck constant, ν is the frequency of the laser radiation, ρ is the density of the microtubule, $x^{\mathrm{Trp/Tyr}}$ is the mass fraction of Trp or Tyr in the microtubule, and M is the molecular mass of the microtubule. This computation results in two-photon absorption coefficients of 4.45922×10^{-17} cm/W and 2.02203×10^{-16} cm/W for Trp and Tyr, respectively. With these values for the two-photon absorption coefficients, the transmitted intensity through a slab of thickness L, $I(L)$, is given by Bhawalkar et al. (1996):

$$I(L) = \frac{1}{L\alpha_2}[\ln(1 + I_0 L\alpha_2)], \tag{7}$$

where I_0 is the incident intensity. At the threshold for microtubule damage, the incident intensities are 1.33×10^9 W/cm^2 and 7.4×10^7 W/cm^2 for ECFP- and EYFP-tagged microtubules, respectively. An upper bound for the slab thickness is double the Rayleigh range of the focused laser beam $2z_0 = 2\pi r_s^2/\lambda = 636\,\mathrm{nm}$. Using $2z_0$ as the slab thickness, the calculated two-photon absorption coefficient given above, and the threshold intensities for microtubule damage, Eq. 7 reveals that the incident and transmitted intensities are essentially equivalent and thus two-photon absorption by the aromatic amino acids within the tagged microtubules cannot provide a mechanism for significant energy deposition.

Another possible mechanism for microtubule damage is the thermal, mechanical, and chemical effects resulting from dielectric breakdown or plasma formation. Recent studies have suggested that the pulse energy and irradiances used in nanosecond microirradiation of cells are sufficient to produce a laser-induced plasma (Rau et al., 2004; Venugopalan et al., 2002) and associated mechanical damage due to the subsequent shock-wave propagation and cavitation bubble dynamics. The threshold of optical breakdown is typically defined by the creation of a density of quasifree electrons of 10^{21} cm^{-3}. When created by picosecond pulses, plasma formation comes about through a combination of multiphoton and cascade ionization processes (Vogel and Venugopalan, 2003). Estimates for the threshold irradiance necessary to produce a plasma using 80-ps laser pulses in otherwise optically transparent media is typically $2–4 \times 10^{11}$ W/cm^2 (Vogel et al., 1996, 1999; Vogel and Venugopalan, 2003). Although these plasma threshold irradiance values are at a minimum 2 orders of magnitude higher than those used to cut the microtubules in this study, there are a few important considerations to bear in mind.

First, there are many data that indicate that the threshold irradiance decreases significantly with increases of focusing angle and all of the measured plasma thresholds were done at focusing angles of only 8–30° (Vogel et al., 1996). This is to be compared with our irradiation conditions at a numerical aperture of 1.4, which corresponds to a focusing angle of ~150°.

Second, these threshold values are for transparent media that possesses no linear optical absorption at the incident wavelength. However, it is well known that the presence of even moderate linear absorption can reduce the threshold irradiance for plasma formation by more than an order of magnitude (Oraevsky et al., 1996). This would also explain the difference in ablation thresholds between ECFP (weak linear absorption) and EYFP (relatively high linear absorption).

Third, the threshold value for plasma formation simply represents the irradiance at which a plasma is formed 50% of the time. Given that in our experiment, 228,000 micropulses are delivered to the target during every macropulse exposure, clearly we can tolerate a much lower probability of plasma formation for a given micropulse to ensure that we produce optical breakdown at some point during the laser exposure macropulse. Assuming that each micropulse can be treated as an independent mutually exclusive event, a new threshold can be calculated that is the irradiance level at which the cumulative probability of plasma formation over N micropulses is 50%. This cumulative probability can be expressed as

$$P(I_{\mathrm{thresh}}^{\mathrm{N}}) = P(I_1 \cup I_2 \ldots \cup I_{\mathrm{N}}) = \sum_{\mathrm{i}=1}^{\mathrm{N}} P(I_{\mathrm{i}}) = N \times P(I_{\mathrm{pulse}}) = 0.5, \tag{8}$$

where $P(\cdot)$ is the probability of plasma formation, $I_{\mathrm{thresh}}^{\mathrm{N}}$ is the cumulative threshold irradiance over N pulses, and I_{i} are the micropulses with irradiance I_{pulse}. Then $I_{\mathrm{thresh}}^{\mathrm{N}}$ is equal to the per-pulse irradiance I_{pulse} such that $P(I_{\mathrm{pulse}}) = 0.5/N$. Given the sigmoidal relationship between irradiance and breakdown probability, it is reasonable to expect $I_{\mathrm{thresh}}^{\mathrm{N}}$ to be orders of magnitude lower than the single-pulse threshold. However, given the lack of experimental data for the picosecond plasma formation at high focusing angles in the presence of significant linear absorption by the fluorescently tagged microtubules, the prospect of plasma formation and the associated thermal and mechanical damage remains a possible mechanism for the observed damage.

Finally, there is gathering evidence that for picosecond and femtosecond pulses, ''low-density plasmas'', i.e., regions with a free-electron density below 10^{21} e^-/cm^3, can be reliably produced at pulse energies below plasma threshold. Although plasma generation with nanosecond pulses is dominated by cascade ionization and leads to the formation of violent plasmas, plasma generation with picosecond pulses involves multiphoton ionization playing an equal, if not dominating, role in plasma generation, which likely facilitates the creation of these low-density plasmas (Vogel et al. 1996, 2002). As the irradiance of the picosecond micropulse is increased, we can see the transition from a localized ablation (Figs. 3 and 5) to a larger reaching ablation (Fig. 4) as the effects of cascade ionization accelerates the plasma formation. Recent computational work has demonstrated that creation of these low-density plasmas produce significant thermal, mechanical, and chemical transients capable of damaging biological structures (Vogel and Noack, 2001; Vogel et al., 2002). Specifically, these calculations suggest that free-electron densities as small as 10^{15} e^-/cm^3, produce thermal, mechanical, and chemical effects capable of intracellular ablation and dissection. Such electron densities can be produced at pulse energies of only 5% of the accepted plasma threshold energy (Vogel et al., 2002).

Thus, even though in this application the threshold irradiance to produce a plasma using 80-ps laser pulses in optically transparent media is 2–4 $\times$ 10^{11} W/cm^2, the laser energy is delivered at a very large numerical aperture and irradiates a fluorescently tagged target with significant linear absorption, both of which will reduce the threshold for plasma formation by as much as an order of magnitude. Moreover, given the probabilistic nature of plasma formation, we require only a subset of the 228,000 micropulses being delivered to the target to provide the observed alteration of microtubules. This combined with the fact that ''low-density plasmas'' can produce damaging thermal, mechanical, and chemical effects to biological structures, we consider that the events connected with ionization and plasma formation represent the most likely candidate for microtubule damage observed in these studies.

Special thanks to the Arnold and Mabel Beckman Foundation Fellow's program for supporting Dr. Botvinick's research.

This work was supported by grants from the United States Air Force (AFOSR no. F9620-00-1-0371) and of the National Institutes of Health (NIH RR 14892).

REFERENCES

Aist, J. R., H. Liang, and M. W. Berns. 1993. Astral and spindle forces in PtK2 cells during anaphase B: a laser microbeam study. *J. Cell Sci.* 104:1207–1216.

Berns, M. W. 1976. A possible two-photon effect in vitro using a focused laser beam. *Biophys. J.* 16:973–977.

Berns, M. W., J. Aist, J. Edwards, K. Strahs, J. Girton, P. McNeill, J. B. Rattner, M. Kitzes, M. Hammer-Wilson, L. H. Liaw, A. Siemens, M. Koonce, et al. 1981. Laser microsurgery in cell and developmental biology. *Science.* 213:505–513.

Berns, M. W., and A. D. Floyd. 1971. Chromosomal microdissection by laser. A cytochemical and functional analysis. *Exp. Cell Res.* 67:305–310.

Berns, M. W., R. S. Olson, and D. E. Rounds. 1969. In vitro production of chromosomal lesions with an argon laser microbeam. *Nature.* 221:74–75.

Berns, M. W., Z. Wang, A. Dunn, V. Wallace, and V. Venugopalan. 2000. Gene inactivation by multiphoton-targeted photochemistry. *Proc. Natl. Acad. Sci. USA.* 97:9504–9507.

Bhawalkar, J. D., G. S. He, and P. N. Prasad. 1996. Nonlinear multiphoton processes in organic and polymeric materials. *Rep. Prog. Phys.* 59:1041–1070.

Calmettes, P. P., and M. W. Berns. 1983. Laser-induced multiphoton processes in living cells. *Proc. Natl. Acad. Sci. USA.* 80:7197–7199.

Carslaw, H. S., and J. C. Jaeger. 1986. Conduction of Heat in Solids. Clarendon Press, New York.

Grill, S. W., P. Gonczy, E. H. Stelzer, and A. A. Hyman. 2001. Polarity controls forces governing asymmetric spindle positioning in the *Caenorhabditis elegans* embryo. *Nature.* 409:630–633.

Joglekar, A. P., H. H. Liu, E. Meyhofer, G. Mourou, and A. J. Hunt. 2004. Optics at critical intensity: applications to nanomorphing. *Proc. Natl. Acad. Sci. USA.* 101:5856–5861.

Khodjakov, A., R. W. Cole, B. F. McEwen, K. F. Buttle, and C. L. Rieder. 1997a. Chromosome fragments possessing only one kinetochore can congress to the spindle equator. *J. Cell Biol.* 136:229–240.

Khodjakov, A., R. W. Cole, and C. L. Rieder. 1997b. A synergy of technologies: combining laser microsurgery with green fluorescent protein tagging. *Cell Motil. Cytoskeleton.* 38:311–317.

Khodjakov, A., C. L. Rieder, G. Sluder, G. Cassels, O. Sibon, and C. L. Wang. 2002. De novo formation of centrosomes in vertebrate cells arrested during S phase. *J. Cell Biol.* 158:1171–1181.

Liang, H., and M. W. Berns. 1983. Establishment of nucleolar deficient sublines of PtK2 (*Potorous tridactylis*) by ultraviolet laser microirradiation. *Exp. Cell Res.* 144:234–240.

Liang, H., W. H. Wright, S. Cheng, W. He, and M. W. Berns. 1993. Micromanipulation of chromosomes in PTK2 cells using laser microsurgery (optical scalpel) in combination with laser-induced optical force (optical tweezers). *Exp. Cell Res.* 204:110–120.

Liang, H., W. H. Wright, C. L. Rieder, E. D. Salmon, G. Profeta, J. Andrews, Y. Liu, G. J. Sonek, and M. W. Berns. 1994. Directed movement of chromosome arms and fragments in mitotic newt lung cells using optical scissors and optical tweezers. *Exp. Cell Res.* 213:308–312.

Liaw, L. H., and M. W. Berns. 1981. Electron microscope autoradiography on serial sections of preselected single living cells. *J. Ultrastruct. Res.* 75:187–194.

McNeill, P. A., and M. W. Berns. 1981. Chromosome behavior after laser microirradiation of a single kinetochore in mitotic PtK2 cells. *J. Cell Biol.* 88:543–553.

Morgenstern, J. P., and H. Land. 1990. Advanced mammalian gene transfer: high titre retroviral vectors with multiple drug selection markers and a complementary helper-free packaging cell line. *Nucleic Acids Res.* 18:3587–3596.

Oraevsky, A. A., L. B. Da Silva, A. M. Rubenchik, M. D. Feit, M. E. Glinsky, M. D. Perry, B. M. Mammini, W. Small IV, and B. C. Stuart. 1996. Plasma mediated ablation of biological tissues with nanosecond-to-femtosecond laser pulses: relative role of linear and nonlinear absorption. *IEEE J. Sel. Top. Quantum Electron.* 2:801–809.

Paltauf, G., and P. E. Dyer. 2003. Photomechanical processes and effects in ablation. *Chem. Rev.* 103:487–518.

Rau, K., A. Guerra III, A. Vogel, and V. Venugopalan. 2004. Investigation of laser-induced cell lysis using time-resolved imaging. *Appl. Phys. Lett.* 84:2940–2942.

Rehms, A., and P. Callis. 1993. Two-photon fluorescence excitation spectra of aromatic amino acids. *Chem. Phys. Lett.* 208:276–282.

Rieder, C. L., R. W. Cole, A. Khodjakov, and G. Sluder. 1995. The checkpoint delaying anaphase in response to chromosome monoorientation is mediated by an inhibitory signal produced by unattached kinetochores. *J. Cell Biol.* 130:941–948.

Sengupta, P., J. Balaji, S. Mukherjee, R. Philip, G. R. Kumar, and S. Maiti. 2001. Determination of the absolute two-photon absorption cross section of tryptophan. *Proc. SPIE.* 4262:336–339.

Skibbens, R. V., C. L. Rieder, and E. D. Salmon. 1995. Kinetochore motility after severing between sister centromeres using laser microsurgery: evidence that kinetochore directional instability and position is regulated by tension. *J. Cell Sci.* 108:2537–2548.

Spurck, T. P., O. G. Stonington, J. A. Snyder, J. D. Pickett-Heaps, A. Bajer, and J. Mole-Bajer. 1990. UV microbeam irradiations of the mitotic spindle. II. Spindle fiber dynamics and force production. *J. Cell Biol.* 111:1505–1518.

Takasone, T., S. Juodkazis, Y. Kawagishi, A. Yamaguchi, S. Matsuo, H. Sakakibara, H. Nakayama, and H. Misawa. 2002. Flexural rigidity of a single microtubule. *Jpn. J. Appl. Phys.* 41:3015–3019.

Tirlapur, U. K., and K. Konig. 2002. Targeted transfection by femtosecond laser. *Nature.* 418:290–291.

Venugopalan, V., A. Guerra III, K. Nahen, and A. Vogel.2002. Role of laser-induced plasma formation in pulsed cellular microsurgery and micromanipulation. *Phys. Rev. Lett.* 88:078103.

Vogel, A., K. Nahen, D. Theisen, and J. Noack. 1996. Plasma formation is water by picosecond and nanosecond Nd:YAG laser pulses. I. Optical breakdown at threshold and superthreshold irradiance. *IEEE J. Sel. Top. Quantum. Electron.* 2:847–860.

Vogel, A., and J. Noack. 2001. Numerical simulation of optical breakdown for cellular surgery at nanosecond to femtosecond time scales. *Proc. SPIE.* 4433:70–80.

Vogel, A., J. Noack, G. Huettmann, and G. Paltauf. 2002. Femtosecond-laser-produced low-density plasmas in transparent biological media: a tool for the creation of chemical, thermal, and thermomechanical effects below the optical breakdown threshold. *Proc. SPIE.* 4633:23–37.

Vogel, A., J. Noack, K. Nahen, D. Theisen, S. Busch, U. Parlitz, D. X. Hammer, G. D. Noojin, B. A. Rockwell, and R. Birngruber. 1999. Energy balance of optical breakdown in water at nanosecond and femtosecond time scales. *Appl. Phys. B-Lasers Opt.* B68:271–280.

Vogel, A., and V. Venugopalan. 2003. Mechanisms of pulsed laser ablation of biological tissues. *Chem. Rev.* 103:577–644.

Walen, K. H., and S. W. Brown. 1962. Chromosomes in a marsupial (*Potorous tridactylis*) tissue culture. *Nature.* 194:406.